



OPEN

High pressure sensor based on intensity-variation using polymer optical fiber

Abdul Ghaffar¹, Fei Ru², Jingming Liu², George Y. Chen³, Jiasheng Ni⁴, Jun Liu¹,
Sadam Hussain¹, Jianping Yu¹, Bhagwan Das⁶ & Mujahid Mehdi⁵

Silica fiber under high pressure increases the risk of fiber breakage or permanent deformation, which may cause sensor failure due to mechanical strength limitations. High pressure can also induce birefringence in optical fiber. In this study, we present a simple design and low-cost high pressure sensor using polymer optical fiber (POF) based on the intensity-variation technique. A side-coupling mechanism in the sensor structure is adopted, which varies the intensity with applied pressure. Two POFs are twisted together to create a sensing region where the light is launched in the first fiber and measurement is taken from the second fiber. In sensing phenomena, cladding mode frustrated total internal reflection occurs when pressure increases. Silicone gel is used in the pressure chamber for sealing and preventing leakage. The sensor structure is able to detect high pressure in the MPa range, where we tested up to 4 MPa. For higher sensitivity, twisted and bend structure is analyzed, and sensitivity is achieved at about 432.21 nW/MPa. However, twisted helical structure is adopted to enhance sensing range which is about 50 cm. The proposed high-pressure sensor structure is easier to fabricate and has high stability because it doesn't require any destructive method as compared to other conventional methods.

Keywords Polymer optical fiber, High-pressure sensor, Coupling method, Intensity-based sensor

High-pressure sensors are critical components in a diverse range of industrial, commercial, scientific applications and advanced aerospace technology. They are designed to measure and monitor pressure levels that are significantly higher than atmospheric pressure^{1,2}. The accurate measurement of high-pressures is essential for operational safety, efficiency, and system integrity in various settings. According to market research from companies like Grand View Research and MarketsandMarkets, the global pressure sensor market is projected to grow from approximately USD 19.66 billion in 2023 to over USD 26.37 billion by 2030, at a compound annual growth rate (CAGR) of about 4.3%³. As technology progresses, the development of even more resilient and accurate high-pressure sensors will continue to propel their indispensability across a wider array of fields, enhancing both economic and operational efficiencies.

Designing pressure sensors based on mechanical systems involves several key elements that utilize mechanical motion to accurately measure pressure changes. Pressure is sensed by mechanical elements such as load cell, strain gauge, bourdon tube, bellows and tactile, and piston and cylinder that are designed and constructed to deflect when pressure is applied⁴. The piston moves within the cylinder according to the applied pressure in piston and cylinder-based pressure sensor⁵. The piston's movement is directly linked to mechanical displays, or it can be converted into electrical signals. Although mechanical pressure sensors offer advantages due to their durability and ease of use in many environments, but their mechanical characteristics introduce limitations that

¹Key Laboratory of Air-Driven Equipment Technology of Zhejiang Province, College of Mechanical Engineering, Quzhou University, 78 North Jihua Road, Quzhou 32400, Zhejiang, China. ²Baoji Cigarette Factory, China Tobacco Shaanxi Industrial Co., Ltd., Baoji, China. ³Guangdong and Hong Kong Joint Research Centre for Optical Fiber Sensors and Key Laboratory of Optoelectronic Devices and Systems of the Ministry of Education and Guangdong Province, College of Physics and Optoelectronic Engineering, Shenzhen University, Shenzhen 518060, China. ⁴Laser Institute, Qilu University of Technology (Shandong Academy of Sciences), Jinan 250014, China. ⁵Faculty of Design, Aror University of Art Architecture Design and Heritage Sindh, Sukkur, Sindh 65200, Pakistan. ⁶Design and Creative Technology Vertical, Torrens University, Ultimo 2007, New South Wales, Australia, Torrens University, New South Wales, Australia. ✉email: 7970930@qq.com; sadamhussain@qzc.edu.cn; mmehdi.faculty@aror.edu.pk

impact accuracy, longevity, and versatility as well as mechanical sensors are usually bulkier in size, complexity in manufacturing, slower response time, mechanical wear and tear, and maintenance requirements.

Designing a pressure sensor based on an electrical system involves utilizing electrical properties such as capacitance⁶, resistance⁷, or inductance⁸ to measure changes in pressure. These sensors provide high accuracy, minimal mechanical movement, and can be easily integrated with modern electronic control systems. Most commonly pressure sensor design is based on capacitive, piezoresistive, piezoelectric and their designs can be customized for various applications^{9–11}. With the advancement of technology, the functions and applications of electrical based pressure sensors are expected to expand, especially with the development of MEMS technology and intelligent sensor systems^{12,13}. However, these sensors have drawbacks like sensitivity to immunity to electromagnetic and radio frequency interference (EMI & FRI), temperature variability, higher costs, and increased complexity make them less suitable for certain environments or cost-sensitive applications.

To avoid conventional sensing system, optical pressure sensors are highly advantageous in environments where high precision, immunity to EMI and FRI, or safety from explosive atmospheres is required^{14,15}. Designing a pressure sensor based on optical systems involves using the properties of light, such as its phase, intensity, or wavelength, to measure pressure changes^{16–18}. However, the fiber optic sensors use the modulation of light transmitted through optical fibers to measure pressure. Changes in pressure alter the light path (phase, intensity, polarization) within the fiber. Typically involves a diaphragm whose deflection under pressure affects the light signal either through physical bending of the fiber or through an interferometric setup where phase shifts are measured^{19–21}. Another method is based on Fabry-Pérot Interferometers which utilize two parallel reflective surfaces forming a cavity (the Fabry-Pérot cavity) whose optical length changes with pressure²². A fiber Bragg grating (FBG) sensor reflects specific wavelengths of light which shift when the fiber is strained by pressure. The grating period of an FBG sensor changes under mechanical strain due to pressure, shifting the reflected wavelength (Bragg wavelength)²³. This wavelength shift is directly related to the pressure applied. However, intensity variation-based sensors have more advantages as compare to other type of sensor as intensity based sensor are suitable, simple, and cost-effective among all other techniques. To further reduce the cost of sensor, polymer optical fiber-based sensor has more advantages^{24,25}. Arnaldo et al.²⁶ reported an intensity variation-based sensor for pressure assessment utilizing highly stretchable POFs fabricated using the light polarization spinning technique. Valente et al.²⁷ reported a hydrostatic pressure sensor using POF based on multimode interferometer. Although the sensor based on intensity variation has relative low-cost as compared to electronic sensor (resistive or capacitive), and the commercially available POF pressure sensor cannot meet the requirements of high-pressure, repetitiveness, and resolution in some sensor applications.

In this study, we worked on optical fiber high-pressure sensor, aiming to avoid any fiber destructive or other traditional techniques. POF is used for sensor structure instead of silica fiber because the POF has higher mechanical strength as compared to silica fiber. Two POF are twisted at certain portion to create a sensing region. In sensing phenomenon, cladding mode frustrated total internal reflection occurs when pressure increased. Three configurations were analyzed among them twisted-bend has higher sensitivity and twisted-helical give wider detection range. The details of sensor structure, sensing mechanism and sensor integration into pressure chamber are given in the next section. The results and discussion are given in the third section.

Materials and methodology

Fiber material and measuring instruments

The optical fiber used in this study was obtained commercially from Mitsubishi. It is important to note that optical fibers come in various types and specifications, and for this study, different diameters were available, ranging from 250 to 3 mm. Among these options, the decision was made to utilize a 1 mm polymer optical fiber known as SK-40, manufactured by Mitsubishi. Several factors influenced this choice. Firstly, the 1 mm POF (SK-40) was selected due to its specific characteristics that are advantageous for the intended application. These include its softness, which facilitates handling and manipulation during experimentation. Additionally, the larger diameter of the fiber compared to other options provides more surface area for interaction, making it suitable for side coupling techniques. Furthermore, the core area of the SK-40 fiber is relatively large i.e., about 980 μm , enhancing its capability for side coupling. This is essential for the experimental setup and ensures efficient transmission of light between fibers. To protect the optical fibers and minimize interference from external light sources, each fiber was covered with a black tube. The covering of the fiber inside the black tube leads to create the barrier against visible light interference, ensuring accurate measurements and reliable experimental results^{28,29}. It's worth noting that the covering of the fiber inside black tube are used at without twisting fibers. Where, the twisted fibers are the sensor section, that are used to uncovered. As the twisted fibers are inside the test section which is already in dark atmosphere. The specifications of the Mitsubishi SK-40 fiber, including details such as core diameter, numerical aperture, and attenuation, are outlined in Table 1. These specifications provide valuable information about the fiber's optical properties such as attenuation, R.I, core cladding diameter which help to understand its behavior in the experimental setup.

For measurement and analysis purposes, optical power meters (PM100USB) containing with S151c as a photodetector, as well as fiber-coupled LED light sources (M660F1), were procured from Thorlabs, USA. These instruments are essential for quantifying the optical power levels and facilitating the generation of light signals necessary for the experiments conducted with the optical fibers. Overall, the choice of optical fiber, along with the protective coating and selection of measurement instruments, was carefully considered to ensure the reliability and effectiveness of the experimental setup for the intended research objectives.

Parameter	Values
Refractive-Index Profile	Step R.I
Clad material	Fluoropolymer
Core Material	Polymethyl Methacrylate (PMMA)
Core diameter	980 μm
Cladding size	10 μm
Transmission attenuation	150 (dB/km)
Refractive-Index	1.49

Table 1. The specification of POF (SK-40) and characteristic parameters.

Sensor's fabrication

As shown in Fig. 1, the sensor structure consists of three distinct configurations: twisted, twisted-bend, and twisted-helical. Each configuration is designed to respond differently to external stimuli, enabling the sensor to detect pressure. The twisted configuration involves simply twisting the optical fiber, while the twisted-bend configuration adds a bending component to the twisted fiber, enhancing its sensitivity to both twisting and bending forces. The twisted-helical configuration takes the twisting concept further by arranging the fiber in a helical pattern, which can offer increased sensitivity. The experimental setup depicted in Fig. 2 is crucial for testing these configurations. It comprises three primary components: a light source, a detector, and polymer optical fibers (POFs). In the experiment, two POFs, each one meter long, were utilized. A specific section of the fiber, spanning from 495 to 505 cm, was designated as the sensing region and subjected to twisting. The use of POFs was deliberate, considering their flexibility, ease of handling, and compatibility with the intended sensing mechanism. The light source emits light into the fiber, which then interacts with the twisted section, causing changes in the light signal that are detected by the detector. These changes can be analyzed to determine the sensor's performance under different conditions.

A twisting structure is strategically employed to facilitate the coupling of radiated power from an illuminating fiber to a second, receiving fiber. This twisting mechanism allows for the optical coupling of light between two parallel fibers, with their cores positioned in close proximity to each other. Unlike conventional fiber setups where a thick cladding serves as a barrier against crosstalk, the chosen coupling method involves the removal of cladding at the coupling point. While this ensures efficient light transfer, it also introduces complexities and fragility, particularly in conventional coupler structures like fused cones and side-polished types. To address these limitations, a resilient twisted structure was adopted in this experiment. This structure enables consistent coupling between the fibers without necessitating complex fabrication processes. Specifically, the uncoated SK-40 fibers were twisted and shielded with a black tube to enhance stability and protect against external interference. Notably, while coated versions of the fibers could be used, they would require the additional step of uncoating the twisting section, adding complexity to the setup.

In the experimental setup, the sensor element designed for pressure sensing was subjected to applied pressure applied to the twisting region. Illumination of the sensor element was achieved using a 660 nm LED source (Thorlabs, M660F1), ensuring consistent and reliable light emission. Pressure readings were correlated with the light intensity captured from the second fiber through an optical power meter. The optical power meter has a precision resolution of 100 pW.

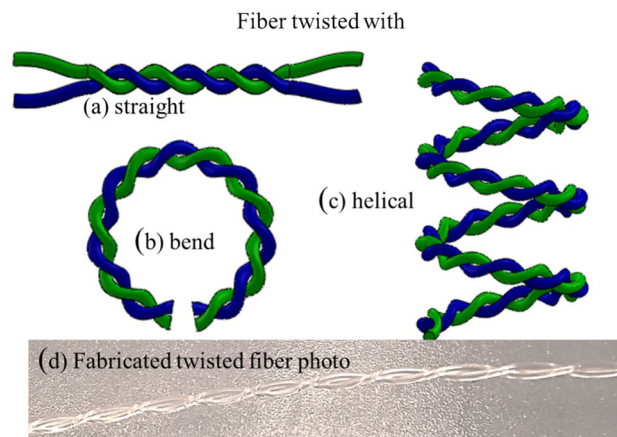


Figure 1. High pressure sensing structure (a) twisted-straight, (b) twisted-bend, and (c) twisted-helical, (d) fabricated twisted sensor photo.

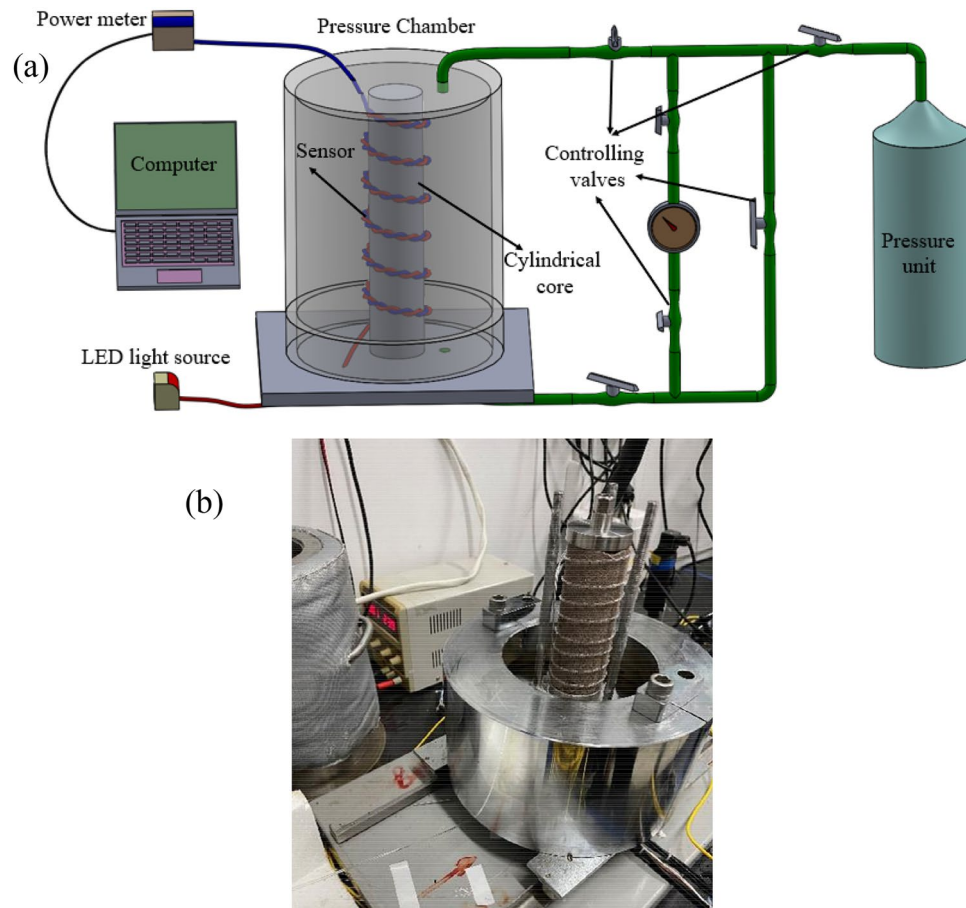


Figure 2. Experimental setup of high-pressure sensor (a) Schematic diagram (b) photo of experimental work.

Sensor integration into pressure chamber

The pressure chamber consists of several parts which include cylindrical core, core-holder inlet, and outlet valves which are used in experiments involving high-pressure conditions. *Cylindrical core*: This is the central piece of the setup, likely where the proposed sensor is attached to it. *Core holder*: A piece that securely holds the cylindrical core in place. It ensures that the cylindrical core remains stationary during the experiment. *Inlet and outlet valves*: These are pathways for the pressure medium (like air) to enter and exit the pressure chamber. The inlet valve allows the medium to come in, while the outlet valve lets it leave. *Sealing and Prevention of Leakage*: to ensure the pressure medium doesn't escape, a fast-curing silicone rubber named KE45-T (made by Shin-Etsu Chemical Co., Ltd.) is used. This substance is applied at the point where fibers enter the chamber. Its role is critical in maintaining the integrity of the system by preventing leaks, which could compromise the experiment's accuracy or safety.

The cylindrical core specimen is placed vertically into the core holder. This orientation and secure placement are crucial for the experiment's accuracy. The sensor is attached to the cylindrical core. It's fixed in place so that it won't shift when high pressure is applied, ensuring reliable readings. Pressure is introduced at the bottom end of the chamber, referred to as downstream. This means the pressure medium flows upward through the chamber, exerting pressure on the cylindrical core.

Pressure unit (Teledyne Isco Inc., Model 100DX) injects pressure into the chamber, allowing for the precise control of pressure. The pressure unit can operate under various injection scenarios, which means it can be programmed to deliver the constant pressures or use adjustable ramps (gradual increases or decreases in pressure) to reach a specified pressure. This flexibility is crucial for experiments requiring precise control over how quickly and how much pressure is applied. The pressure inside the chamber, both for injection and outflow, is meticulously regulated. The pressure unit ensures the desired pressure is achieved and maintained during injection. To monitor and measure the pressures accurately, three pressure transducers (Baumer Pressure Transmitter, series Y912 53B) are employed. These transducers have a high accuracy of $\pm 0.3\%$ Full Scale (FS) at 20 °C, meaning they can detect very slight changes in pressure with minimal error. Two of these transducers are placed at the inlet, where the pressure enters the chamber, to measure incoming pressures. The third is placed at the outlet, where fluid exits the chamber, to ensure that the pressure control systems are working as intended and to monitor the experiment's effect on pressure changes. So, this setup allows for highly controlled experiments involving pressure changes within a chamber. The components work together to ensure the core specimen is properly subjected to pressure while measurements are taken without any interference from leaks or sensor movement. For the response time analysis of the final configuration, the pressure is meticulously regulated using the pressure unit

to apply and maintain the desired pressure levels. The monitoring system ensures that any changes in pressure are accurately recorded, enabling us to analyze the sensor's response time under controlled conditions.

Sensor's working principle

In the described structure, optical power coupling is achieved through the twisting of two fibers. However, when the fiber is subjected to both twisting and bending, the behavior of light within the fiber changes. Initially, light propagating through the fiber core begins to leak out as a result of refraction and tunneling mechanisms induced by the twisting and bending. In single-mode optical fibers, calculations are often simplified by considering the thickness of the cladding to be infinite. By streamlining the process, we can focus on a single reflection occurring at the boundary between the core and cladding, which eliminates any escaped light at that point. Nonetheless, light that manages to escape at the core-cladding boundary might bounce back into the core upon hitting the cladding-external environment interface. Much like the initial reflection, if light doesn't fulfill the criteria for total internal reflection at this second interface, it will be refracted, rapidly losing energy and ultimately being emitted as radiation. Tunneling light, on the other hand, is formed from light that satisfies the conditions for total internal reflection but experiences slow leakage due to the tunneling mechanism within the cladding.

A key difference emerges between the tunneling rays at the core-cladding boundary and those at the juncture of cladding and the external medium: the latter's evanescent field invades the adjacent material via a process called frustrated total internal reflection (FTIR). Loss of light intensity in this context is heavily influenced by the refractive index of the ambient medium. FTIR, or the frustrated total internal reflection phenomenon, arises when some cladding mode, contained within an optical fiber, migrates from the fiber cladding to the outside world following an encounter or near-collision with another medium (labeled medium 3), distinct in refractive index from the cladding itself (medium 2). This specific instance is labeled cladding mode frustrated total internal reflection (CMFTIR) and holds substantial sway over the operational characteristics of optical fibers.

When a twisted fiber experiences perturbation, such as finger touch, force, or applied pressure (as depicted in Fig. 3), the effect of CMFTIR leads to a loss of light, resulting in a decline in coupled power that can be observed by measuring the intensity. Straight fibers confine optical energy predominantly within the core, minimizing energy transmission to the cladding environment interface. Moreover, the thick cladding and outer coating of glass fibers shield the energy field from external influences. For these reasons, POFs such as SK-40, which typically lack coating and feature a thin cladding, are preferred for sensor structures where the CMFTIR effect is of interest. POFs facilitate the observation of CMFTIR effects due to their uncoated nature and thinner cladding, making them more sensitive to external perturbations and refractive index changes. This sensitivity enhances the sensor's responsiveness and effectiveness in detecting variations in the surrounding environment, making it a suitable choice for applications where precise monitoring and detection are required.

Testing procedure

The testing procedure described involves a series of experimental evaluations of a sensor after it has been fabricated and integrated into a pressure chamber. Below is a detailed technical explanation of the testing procedure:

1. *Integration and Initial Testing:* the sensor's fabrication is installed within a pressure chamber and pressure is applied into the chamber. The initial phase of testing focuses on evaluating the sensor's real-time response. This involves monitoring how the sensor reacts to changes in pressure in both bent and unbent (straight) configurations. Then the sensor's performance was evaluated under physical stress, where the sensing length was intentionally increased.
2. *Comprehensive Characterization:* the testing procedure extends beyond initial response which encompasses: measurement response, repeatability response, bending effect, and sensitivity response. Further analysis of how bending influences the sensor's performance, including any potential degradation or alteration in sensitivity.
3. *Sensing Length and Helical Structure:* An important aspect of the sensor's design is its sensing length, particularly the implementation of a helical structure. This design choice is discussed in the context of enhanc-

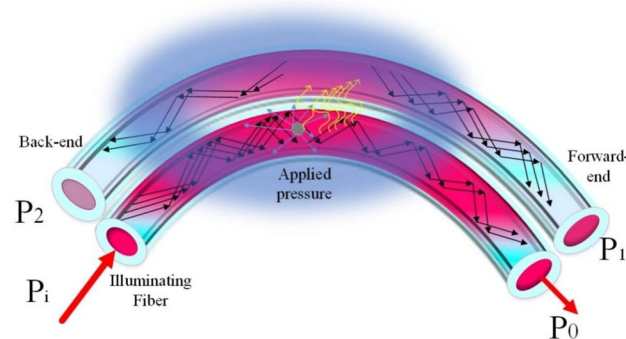


Figure 3. Schematic diagram of sensing mechanism of pressure sensor.

ing the sensor's sensing region. The helical structure likely increases the surface area exposed to pressure changes, potentially improving the sensor's sensitivity and effectiveness. This structural adaptation is crucial for applications requiring high sensitivity and accurate humidity measurement over a larger area or volume within the chamber.

Results and discussion

The pressure sensor is analyzed on three configurations—twisted-straight, twisted with-bend, and helical that all implemented using a single POF (SK-40). The fiber has a core diameter of $980 \pm 10 \mu\text{m}$ and a cladding diameter of $1000 \pm 10 \mu\text{m}$ made of Polymethyl methacrylate (PMMA) fibers. The POF has impressive mechanical properties, like $\sim 124 \text{ MPa}$ compressive yield strength, $\sim 83.4 \text{ MPa}$ tensile yield strength, and $\sim 3.3 \text{ GPa}$ Young's modulus^{30,31}. Compared to silica fibers, POF excels in flexibility and elasticity, allowing tighter bends and larger strain before breaking. This makes POF a champion in mechanically demanding environments. A pressure is applied into the pressure chamber unit, targeting the central section of the POF, inducing internal pressure within the fiber.

When pressure is applied to the sensor, there is a noticeable decrease in output power from an initial power (P1) to a reduced power (P2) as shown in Fig. 4. This decline in power is attributed to changes in the light propagation characteristics within the optical fiber. Meanwhile, change in coupled power shows that sensor is able to detect the effect pressure, and can be used as pressure sensor. In theory, optical fibers are described as having an infinite cladding layer. Light rays hitting the core-cladding interface are refracted (bent) and, under the assumption of infinite cladding, are considered to be lost indefinitely. Practically, the cladding in optical fibers serves as a waveguide. While it's theoretically assumed that light refracted at the core-cladding interface is lost, in reality, some of these light rays can be reflected back into the core from the interface between the cladding and the external environment. The ability of light rays to be reflected into the core is significantly influenced by the R.I of the external environment surrounding the cladding. Changes in the external R.I can affect the number of light rays that are reflected.

Applying pressure to the fiber sensing region alters its external environment, potentially changing the R.I to match or even exceed that of the fiber's cladding (for example, the cladding of SK40 with an RI of 1.402). Such changes can compromise the cladding's ability to achieve total internal reflection (TIR), a critical mechanism for keeping light within the core as it travels along the fiber³². When TIR is disrupted or limited, light that would normally be reflected back into the core at the cladding-environment interface is lost. The passage mentions "CMFTIR" effect which could be referring to a critical mechanism, where TIR is compromised. When the external R.I approaches that of the cladding, the conditions for TIR are not met, leading to light loss and, consequently, a decrease in output power as observed in Fig. 4.

The critical mode for total internal reflection effect typically does not significantly influence the in single optical fibers, as the external R.I minimally impacts the power modulated within the cladding modes. To modify these cladding modes and thereby study their properties, certain techniques such as the creation of literal sections³³, tapering³⁴, or bending of the fibers are employed³⁵. Our research focused on evaluating the CMFTIR effect under twisted structure and analyze on three distinct conditions: twisted-straight, twisted-bend, and twisted-helical. This approach aimed to comprehensively understand how pressure influences sensor, particularly considering the CMFTIR effect. It has been established that the CMFTIR effect can lead to a loss of optical power in certain cladding modes when an uncoated fiber's cladding is disturbed by external pressure. The response of pressure sensor depicted in Fig. 3 and observed a decrease in output power. The decrease in output power is caused by CMFTIR.

Figure 4 indicates that sensor exhibits a power drop when subjected to different pressure levels, indicating the occurrence of the CMFTIR effect in such twisting region. In contrast, twisted optical fibers show a pronounced CMFTIR effect because the twisting alters the mode-field distribution, creating multiple cladding modes. This structural modification enhances the fiber's sensitivity to external pressure, as evidenced by the power reduction figures provided: approximately 40% without bending, and 75% with bending (calculated by $n = p/p_z$).

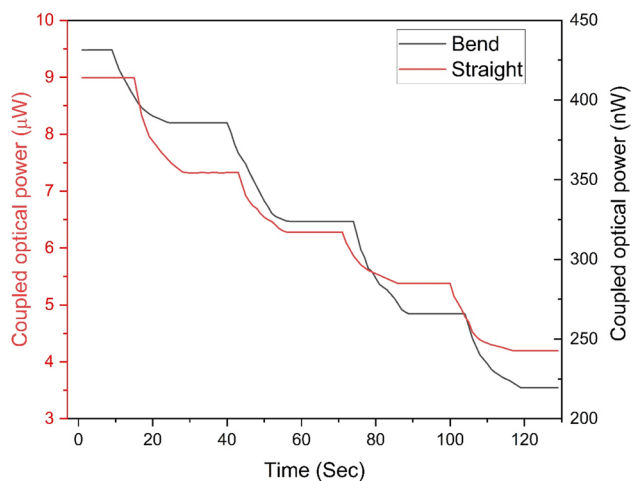


Figure 4. The pressure sensor response with twisted-straight and twisted-bend.

These reductions in light transmission efficiency highlight the effectiveness of the twisted design in amplifying the CMFTIR effect, where the proportion of cladding modes which are more susceptible to environmental changes than the core mode increases significantly. However, despite this increase, the power carried by the cladding modes remains relatively low compared to the light source's power, indicating that while the sensitivity is enhanced, it is still a fraction of the total power capacity of the fiber.

Correlation and differential detection methods were employed to enhance the signal-to-noise ratio of the system in the few studies^{36,37}. A lock-in amplifier played a crucial role in facilitating the correlation operations needed to isolate a faint signal from overwhelming noise. Consequently, depending solely on the bending effect proved inadequate for optimal sensing applications. Instead, this research demonstrated that incorporating a twist in the fiber markedly improved the CMFTIR effect. The pressure sensor measurement response is shown in Fig. 5. Here, as the applied pressure on the sensor structure ranged from 0 to 4 MPa, a noticeable reduction in coupled power was observed, correlating with the initial power coupling in the dual twisted fibers and the subsequent intensity drop as the pressure escalated, attributable to the CMFTIR effect. The response curve depicted in Fig. 5 maintains considerable linearity, with the correlation coefficients (R^2) for the curves being nearly perfect at 0.9957 and 0.9975, respectively.

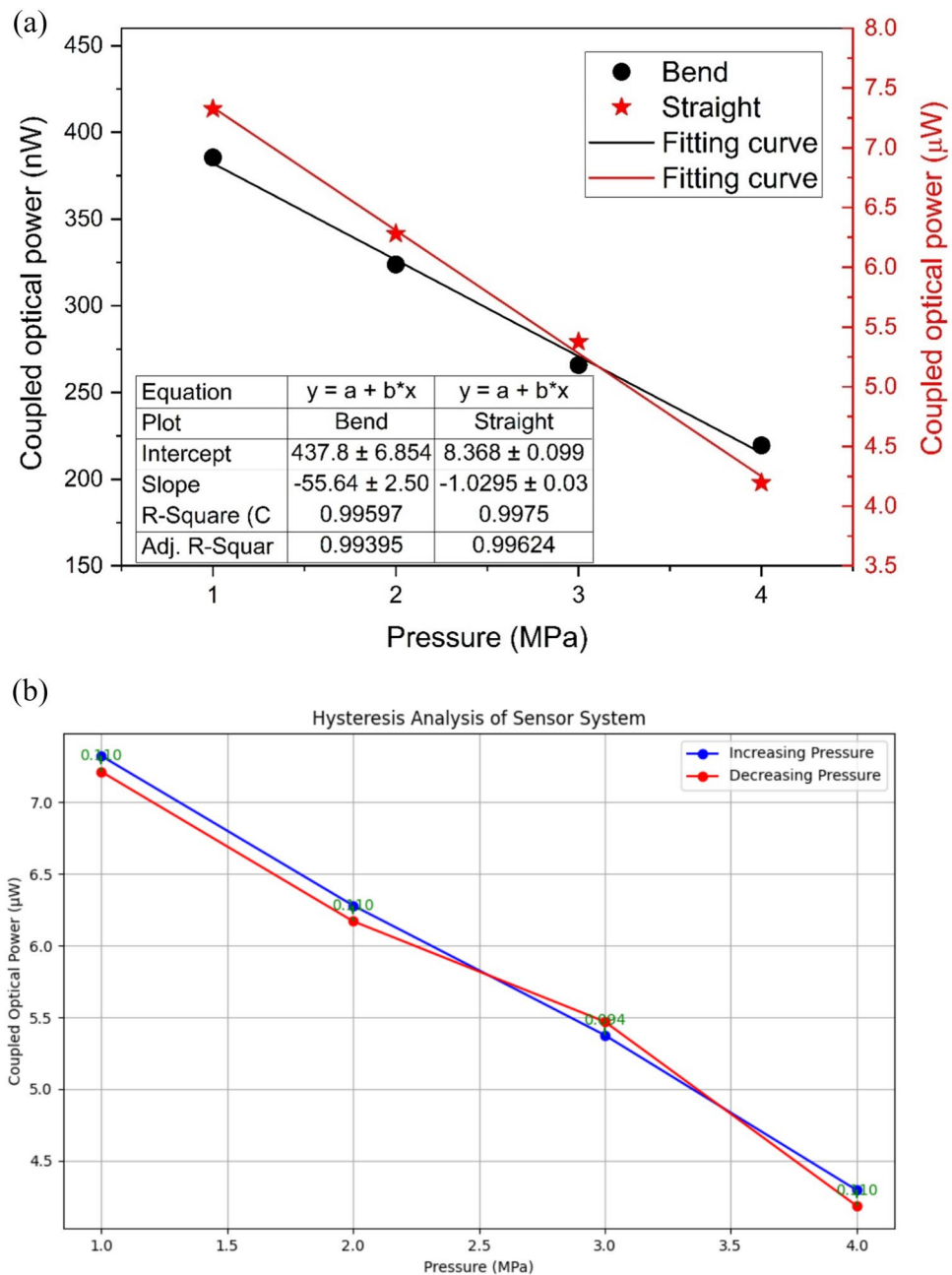


Figure 5. Pressure sensor's measurement response. (a) Measured response with straight and bend condition, (b) hysteresis analysis.

The findings show that the sensor maintains a high degree of linearity which is analyzed in straight and bend configuration, with minimal deviation from the ideal straight-line behavior, thereby ensuring reliable measurements. On the other hand, hysteresis describes the difference in the sensor's output when the input pressure is increasing versus when it is decreasing. This parameter is crucial because significant hysteresis can lead to errors and inconsistencies in measurements. We have quantified the hysteresis in our sensor by comparing the coupled optical power during increasing and decreasing pressure cycles. The results indicate that the sensor exhibits minimal hysteresis, which is approximately $0.236 \mu\text{W}$, demonstrating its capability to provide consistent readings regardless of the direction of pressure change.

The results in Fig. 6 show the response of pressure sensor test conducted four times to assess its repeatability. Critical evaluation of these results indicates that the sensor exhibits consistent behavior across multiple trials, as evidenced by the overlapping data points for each iteration labeled as 1st, 2nd, 3rd, and 4th. The near convergence of these points suggests there is no significant variance in the sensor's response to pressure, implying high reliability and precision of the sensor's performance. The coupled optical power, which likely correlates to applied pressure, maintains a consistent decremental trend as pressure increases. This consistency across trials confirms the repeatability of the sensor, which is crucial for practical applications where sensors must perform reliably over many cycles.

The sensor operates based on intensity modulation, where changes in input power significantly impact sensor performance. Figure 7 shows the sensor's response under different input powers. The bar chart presents a comparative analysis of a sensor's performance under different initial light power levels (6 mW, 12 mW, and 18 mW),

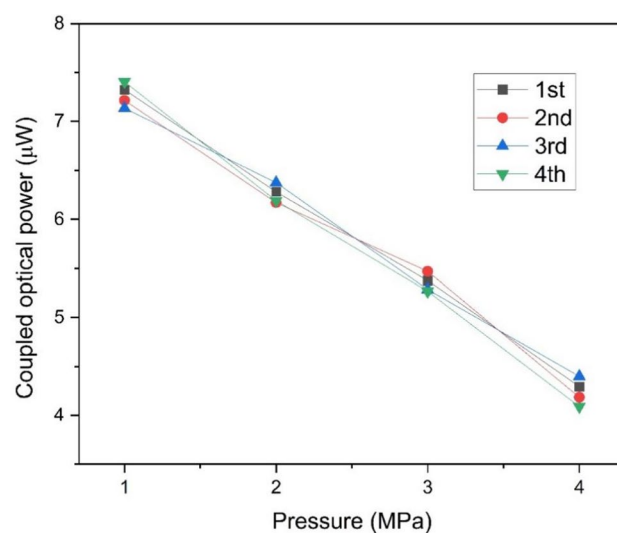


Figure 6. Repeatability response of pressure sensor.

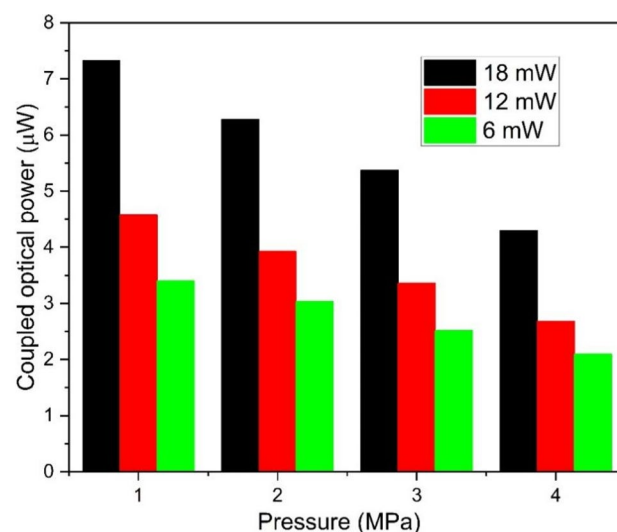


Figure 7. The effect of different initial power on sensor's performance.

mW) when subjected to varying pressures (1–4 MPa). The vertical axis indicates the coupled optical power in the second, and the horizontal axis represents the pressure applied. As shown in Fig. 7, the coupled optical power decreases with increasing pressure across all initial power settings, which is a typical response in pressure sensing applications. It is worth noticing that the influence of the input power setting on effect on sensitivity of sensor. At lower pressures (1 MPa), the difference in coupled optical power is more pronounced between the various input power levels. However, as the pressure increases, the disparities in response diminish. This suggests that higher input powers may provide stronger signal intensities initially, but under high intensity, the sensor's ability to maintain these differences is compromised, possibly due to the physical limitations of the fiber or saturation effects. This trend could imply that while higher initial powers might offer better performance at lower pressures, the benefits reduce under higher pressure conditions. This relationship highlights the importance of stable input power to ensure consistent sensor performance and minimize the effects of power source fluctuations and macro-bending on the sensor's accuracy and reliability.

In the second configuration twisted fiber is bent where it affects the coupled optical power in response to different pressure levels. Diverse cylindrical cores with varying diameters were utilized, around which the sensor was coiled to investigate the sensor's responsiveness is affected by changes in the bend radius. Figure 8 illustrates the impact of varying bending radii on a sensor's performance. The bending radii are represented by different lines for 5 mm, 10 mm, 20 mm, and 30 mm. The trend shows that as the bending radius increases, the sensor's response to pressure (in terms of coupled optical power) diminishes, with the steepest drop shown in the smallest radius (5 mm) and the shallowest in the largest radius (30 mm). This indicates that the optical fiber is more sensitive to pressure changes when bent at tighter radii. The optical power coupling is stronger in tightly bent fibers because bending can cause more light to escape from the core into the cladding or the surrounding environment, and this effect is amplified under pressure. The overall bending effect analysis is shown in Table 2. In contrast, fibers bent at larger radii retain more of the light in the core, resulting in less pressure-induced loss of optical power. For applications where high sensitivity to pressure is desired, a smaller bending radius would be preferable. However, for stability and durability, or where a more gradual response to pressure is needed, a larger bending radius may be advantageous. This data is crucial for designing fiber optic sensors tailored to specific measurement needs and environments.

Helical structure for wide range sensing region

In the previous section, we found that twisting length could be increased. As mentioned in section two, 10 cm fiber was twisted and there is detection if force/pressure applied at any point in between twisting section. The twisting length was further increased up to 50 cm and wound in helical shape on the cylindrical core. The

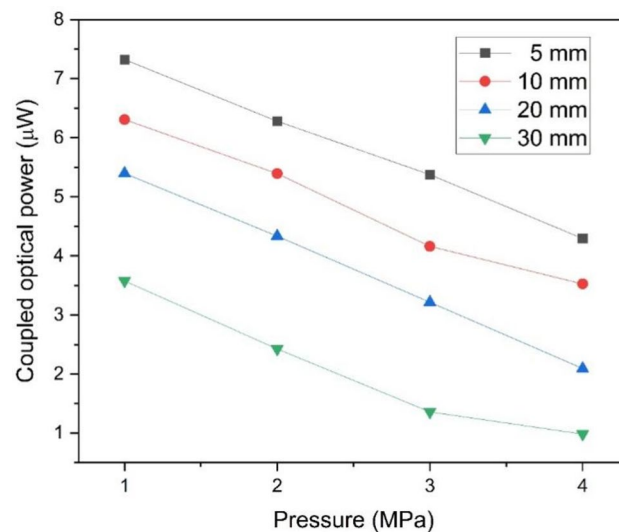


Figure 8. Bending radius effect on sensor response.

No.	Bend radius (mm)	$y = ax + b$	Sensitivity nW/Mpa	R^2
1	5	$- 55.64x + 437.8$	432.2	0.996
2	10	$0.9579x + 7.2429$	586.2	0.9868
3	20	$- 1.1028x + 6.5181$	713.2	0.9898
4	30	$- 0.9627x + 4.4288$	825.7	0.9846

Table 2. Bending radius effect on sensor performance.

experimental setup's photo is shown in Fig. 2. When pressure is applied, constant pressure is inserted to the whole sensing region. As a result, coupled power in second fiber was decreasing. However, we have evaluated that sensor able to detect pressure at any point and adopted an alternative method to apply the pressure on different points of sensor. The thumb was used to apply the pressure and analyze the sensor response. As shown in Fig. 9, the sensor detects the applied pressure effect and the pressure applied to five different points. The sensor detects the effect of pressure whenever pressure is applied to any point of the sensor. This helical configuration could be customized depending upon the specific application where wide range detection range is required.

A performance comparison with proposed sensor is shown in Table 3. The straight configuration of the sensor demonstrates significantly higher stability and less fluctuation compared to the bend configuration. However, the bend configuration offers greater sensitivity, as shown by various analyses of different bend configurations (see Fig. 8). As the bend radius decreases, the sensor's sensitivity increases due to more radiation power emerging from higher bending radii, which ultimately reduces the coupled intensity. The helical configuration, on the other hand, combines the advantages of both the straight and bend configurations. It not only extends the sensing length but also provides a balanced performance by merging the high stability of the straight configuration with the enhanced sensitivity of the bend configuration. The bend configuration is the most consistent and sensitive among the three configurations. This configuration is found to be most suitable, making it the preferred choice for precision pressure sensing applications. However, sensitivity can be further optimized by applying specialized coatings to the fiber surface that can amplify the enhance the coupling power, thus increasing sensitivity. Such coating could be agarose gel and other chemicals materials.

Conclusion

In this research work, a low-cost, easy to fabricate optical fiber high-pressure sensor is reported based on intensity-variation technique. The polymer optical fiber was used to fabricate the sensor. The sensor structure is based on twisting of two POF where is light was launched in first fiber and measurement was taken from the second fiber based on coupled intensity. When pressure was applied, the coupled intensity was changing due to CMFTIR effect. In the first approach, the sensor's response was analyzed with twisted-straight structure, sensor's sensitivity was enhanced in twisted-bend structure. In the last approach, twisted-helical structure was adopted to enhance the sensing length. The applied pressure was about 4Mpa. However, the sensor range could be enhanced

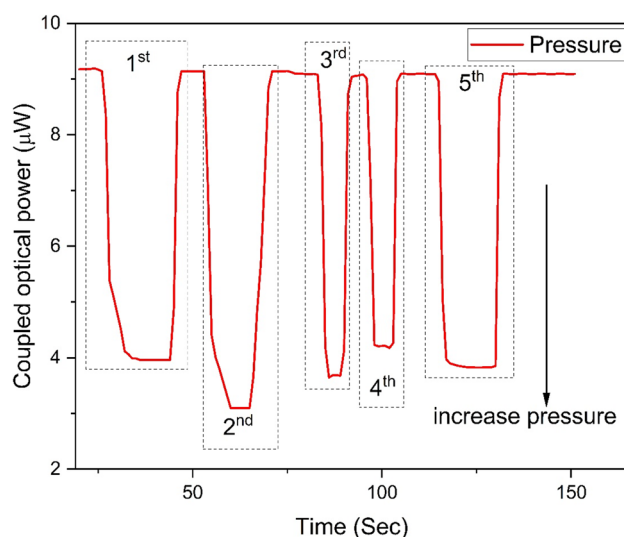


Figure 9. Response of pressure sensor in helical structure for wide sensing range.

References	Method	Sensitivity	Range	Type of Fiber
18	Fabry-Pérot	~2.2 nm/kPa	15 psi	SOF
19	Fabry-Pérot	705.64 μm/MPa	0–0.1 MPa	SOF
20	Fabry-Pérot	28.6 mV/Pa	2.8 Pa	SOF
22	Fabry-Pérot	1.598 μm/MPa	1 MPa	SOF
23	Fiber Bragg gratings	0.06 nm/psi	50 psi	SOF
26	Intensity modulation	143.21 ADC/kPa,	4.6 kPa	POF
This work	Intensity modulation (based on CMFTIR)	421 nW/MPa	4 MPa	POF

Table 3. A performance comparison with proposed sensor.

as the sensor is able to detect a wide range of detection and we have demonstrated sensing length about 50 cm. Twisted-helical structure is highlight for wide range of sensing region. Furthermore, different configurations of sensor could be optimized depending on requirements. This high-pressure sensor is low-cost as compared to other methods because this pressure sensor requires an LED, power meter and few meters of polymer optical fiber. Furthermore, the taper method will be introduced to analyze the sensor sensitivity and multiplexing method will be adopted in future work.

Data availability

Data will be available on request from corresponding authors.

Received: 24 May 2024; Accepted: 31 July 2024

Published online: 10 August 2024

References

- Mishra, R. B. *et al.* Recent progress on flexible capacitive pressure sensors: From design and materials to applications. *Adv. Mater. Technol.* **6**(4), 2001023 (2021).
- Ruth, S. R. A. *et al.* Microengineering pressure sensor active layers for improved performance. *Adv. Funct. Mater.* **30**(39), 2003491 (2020).
- Pressure Sensor Market Size & Trends <https://www.grandviewresearch.com/industry-analysis/pressure-sensors-industry>.
- Jena, S. & Gupta, A. Review on pressure sensors: A perspective from mechanical to micro-electro-mechanical systems. *Sens. Rev.* **41**(3), 320–329 (2021).
- Wang, X. S. & Chen, X. S. Measuring radial pressure distributions of piston rings based on partial-thin-walled cylinder. *Measurement* **43**(2), 197–203 (2010).
- Ha, K. H. *et al.* Soft capacitive pressure sensors: Trends, challenges, and perspectives. *ACS Nano* **16**(3), 3442–3448 (2022).
- Vijayababu, M. & Chintagumpala, K. Review of MXene-based resistance pressure sensors for vital signs monitor. *J. Electron. Mater.* **51**(4), 1443–1472 (2022).
- Wang, Y. Z., Qu, H. Q. & Diao, S. Flexible inductance pressure sensor for wearable electronic devices. *J. Nanoelectron. Optoelectron.* **18**(6), 652–662 (2023).
- Yu, C. X. *et al.* High-performance multifunctional piezoresistive/piezoelectric pressure sensor with thermochromic function for wearable monitoring. *Chem. Eng. J.* **459**, 141648 (2023).
- Kurnaz, S. *et al.* The Parylene C as a flexible substrate and passivation layer: A Promising candidate for a piezoelectric, piezoresistive, and capacitive pressure sensor in low-pressure range. *Ieee Sens. J.* **23**(19), 22277–22284 (2023).
- Luo, J. J. *et al.* Highly sensitive, wide-pressure and low-frequency characterized pressure sensor based on piezoresistive-piezoelectric coupling effects in porous wood. *Carbohydr. Polym.* **315**, 120983 (2023).
- Simsek, E. *et al.* High-pressure deflection behavior of laser micromachined bulk 6H-SiC MEMS sensor diaphragms. *Sens. Actuat. Phys.* **162**(1), 29–35 (2010).
- Mousavi, M., Alzgoool, M. & Towfighian, S. A MEMS pressure sensor using electrostatic levitation. *Ieee Sens. J.* **21**(17), 18601–18608 (2021).
- Chu, C. L., Wang, J. J. & Qiu, J. Y. Miniature high-frequency response, high-pressure -range dynamic pressure sensor based on all-silica optical fiber Fabry-perot cavity. *Ieee Sens. J.* **21**(12), 13296–13304 (2021).
- Rosolem, J. B. *et al.* Techniques and materials for optical fiber sensors sealing in dynamic environments with high pressure and high temperature. *Sensors* **21**(19), 6531 (2021).
- Vorathin, E. *et al.* Review of high sensitivity fibre-optic pressure sensors for low pressure sensing. *Opt. Laser Technol.* **121**, 105841 (2020).
- Chen, Z. *et al.* Pressure sensor based on optical resonator in a compact plasmonic system. *Ieee Sens. J.* **24**(4), 4418–4423 (2024).
- Dai, G. *et al.* Perovskite quantum dots based optical Fabry-perot pressure sensor. *ACS Photon.* **7**(9), 2390–2394 (2020).
- Zhu, J. L. *et al.* An optical fiber Fabry-Perot pressure sensor using corrugated diaphragm and angle polished fiber. *Opt. Fiber Technol.* **34**, 42–46 (2017).
- Wang, X. D. *et al.* Diaphragm design guidelines and an optical pressure sensor based on MEMS technique. *Microelectron. J.* **37**(1), 50–56 (2006).
- Zeng, N. *et al.* Diaphragm-type fiber-optic interferometric acoustic sensor. *Opt. Eng.* **42**(9), 2558–2562 (2003).
- Ma, W. Y. *et al.* Microelectromechanical system-based, high-finesse, optical fiber Fabry-Perot interferometric pressure sensors. *Sens. Actuat. Phys.* **302**, 111795 (2020).
- Ahmad, H. *et al.* High-sensitivity pressure sensor using a polymer-embedded FBG. *Microw. Opt. Technol. Lett.* **50**(1), 60–61 (2008).
- Ghaffar, A. *et al.* An enlarge polymer optical fiber linear-displacement sensor based on constructive interference. *Opt. Fiber Technol.* **63**, 102481 (2021).
- Shi, J. *et al.* Dynamic rotational sensor using polymer optical fiber for robot movement assessment based on intensity variation. *Polymers* **14**(23), 5167 (2022).
- Leal, A. *et al.* Low-cost and high-resolution pressure sensors using highly stretchable polymer optical fibers. *Mater. Lett.* **271**, 127810 (2020).
- Valente, N. F., Bilro, L. & Oliveira, R. Hydrostatic pressure sensor based on polymer optical fiber multimode interferometer. *Ieee Sens. J.* **23**(12), 12876–12880 (2023).
- Ghaffar, A. *et al.* A simple and high-resolution POF displacement sensor based on face-coupling method. *Measurement* **187**, 110285 (2022).
- Hu, Y. *et al.* A narrow groove structure based plasmonic refractive Index sensor. *IEEE Access* **8**, 87289–87295 (2020).
- Yang, D. X. *et al.* Structural and mechanical properties of polymeric optical fiber. *Mater. Sci. Eng. A* **364**(1), 256–259 (2004).
- Ghaffar, A. *et al.* Analysis of force sensor using polymer optical fiber based on twisting structure. *IEEE Sens. J.* **22**(24), 23960–23967 (2022).
- Zanoon, N. I. The phenomenon of total internal reflection and acceleration of light in fiber optics. *Int. J. Comput. Appl.* **975**, 8887 (2014).
- Leal-Junior, A. G., Frizzera, A. & Pontes, M. J. Sensitive zone parameters and curvature radius evaluation for polymer optical fiber curvature sensors. *Opt. Laser Technol.* **100**, 272–281 (2018).
- Zhang, W. *et al.* Advances in tapered optical fiber sensor structures: From conventional to novel and emerging. *Biosensors* **13**(6), 644 (2023).
- Ghaffar, A. *et al.* Two-dimensional displacement optical fiber sensor based on macro-bending effect. *Opt. Laser Technol.* **120**, 105688 (2019).
- Wang, D. *et al.* Distributed optical fiber low-frequency vibration detecting using cross-correlation spectrum analysis. *J. Lightw. Technol.* **38**(23), 6664–6670 (2020).

37. Qin, Z., Chen, H. & Chang, J. Signal-to-noise ratio enhancement based on empirical mode decomposition in phase-sensitive optical time domain reflectometry systems. *Sensors* 17(8), 1870 (2017).

Acknowledgements

This research was supported by the Joint Funds of the Zhejiang Provincial Natural Science Foundation of China under Grant No. LZ Y24E050002, Quzhou Science and Technology Planning Project, Grant No. 2023K231.

Author contributions

Formal analysis, M.M., F.R., J.L. and B.D.; Funding acquisition, L.J.; Investigation, M.M., G.Y.C.; Methodology, S.H. and Y.P.; Validation and Review, G.Y.C., J.N.; Writing—original draft A.G.

Competing interests

The authors declare no competing interests.

Additional information

Correspondence and requests for materials should be addressed to J.L., S.H. or M.M.

Reprints and permissions information is available at www.nature.com/reprints.

Publisher's note Springer Nature remains neutral with regard to jurisdictional claims in published maps and institutional affiliations.

Open Access This article is licensed under a Creative Commons Attribution-NonCommercial-NoDerivatives 4.0 International License, which permits any non-commercial use, sharing, distribution and reproduction in any medium or format, as long as you give appropriate credit to the original author(s) and the source, provide a link to the Creative Commons licence, and indicate if you modified the licensed material. You do not have permission under this licence to share adapted material derived from this article or parts of it. The images or other third party material in this article are included in the article's Creative Commons licence, unless indicated otherwise in a credit line to the material. If material is not included in the article's Creative Commons licence and your intended use is not permitted by statutory regulation or exceeds the permitted use, you will need to obtain permission directly from the copyright holder. To view a copy of this licence, visit <http://creativecommons.org/licenses/by-nc-nd/4.0/>.

© The Author(s) 2024